

Article

Precise Analysis of the Differences in the Laser-Activated Energy Density of Aluminum Nitride Ceramics under Various Gas Bath Environments

Haitao Zhang ^{1,2}, Yingming Wang ³, Jing Shao ^{3,*} , Hao Dong ³, Zhiyuan Sun ⁴, Suli Han ³ , Changqing Xie ^{1,2}, Ping Song ⁵, Shufeng Sun ^{3,*}  and Zhenwei Nie ⁶

- ¹ Key Laboratory of Microelectronic Devices & Integrated Technology, Institute of Microelectronics, Chinese Academy of Sciences, Beijing 100029, China; zhanght@sklao.ac.cn (H.Z.); xiechangqing@imec.ac.cn (C.X.)
² School of Integrated Circuits, University of Chinese Academy of Sciences, Beijing 100049, China
³ Shandong Collaborative Innovation Center of Laser Green Intelligent Manufacturing Technology and Equipment, Qingdao University of Technology, Qingdao 266520, China; qlwym1998@gmail.com (Y.W.); sdawdjhh@163.com (H.D.); best_hsl@163.com (S.H.)
⁴ Beijing Institute of Control Engineering, Beijing 100094, China; biceszy@sina.com
⁵ Ceyear Technologies Co., Ltd., No. 98, Xiangjiang Road, Huangdao District, Qingdao 266000, China; songping@ceyear.com
⁶ Changchun Institute of Optics, Fine Mechanics and Physics, Chinese Academy of Sciences, Changchun 130033, China; niezhenwei@hotmail.com
* Correspondence: qunying12@163.com (J.S.); shufeng2001@163.com (S.S.)

Abstract: Laser activation can lead to the formation of a layer of aluminum on the surface of aluminum nitride ceramics, thereby preparing metal circuits. Under various gas environments, there are differences in the aluminum layers precipitated by laser-activated aluminum nitride ceramics. The existing literature uses the width of the metal layer to characterize this difference, and these data are very imprecise. Usually, laser energy density is used to describe this processing difference. However, the existing concept of laser energy density is an average value and is not suitable for the threshold of laser activation, because the intensity gradient of the focused Gaussian beam is large, and different intensity distributions represent different energy levels. This article applied a precise concept of laser energy density that sees it as being proportional to light intensity and can be used to evaluate the difference in laser energy density required for the decomposition of aluminum nitride ceramics under various gas bath conditions precisely. Due to the strong energy of a focused Gaussian beam, it is not possible to directly obtain the intensity distribution. Here, the intensity distribution of the collimated beam was used to indirectly obtain the intensity distribution of the focused Gaussian beam, and the threshold values for laser activation under different gas baths were calculated. It was found that the minimum energy density in air increased by 12.5%, and the minimum energy density in nitrogen increased by 3%, using the minimum energy density required for laser activation in argon as the reference.

Keywords: aluminum nitride ceramics; laser-activation; energy density; gas bath environments



Citation: Zhang, H.; Wang, Y.; Shao, J.; Dong, H.; Sun, Z.; Han, S.; Xie, C.; Song, P.; Sun, S.; Nie, Z. Precise Analysis of the Differences in the Laser-Activated Energy Density of Aluminum Nitride Ceramics under Various Gas Bath Environments. *Coatings* **2024**, *14*, 624. <https://doi.org/10.3390/coatings14050624>

Academic Editor: Csaba Balázs

Received: 6 April 2024

Revised: 3 May 2024

Accepted: 11 May 2024

Published: 15 May 2024



Copyright: © 2024 by the authors. Licensee MDPI, Basel, Switzerland. This article is an open access article distributed under the terms and conditions of the Creative Commons Attribution (CC BY) license (<https://creativecommons.org/licenses/by/4.0/>).

1. Introduction

Aluminum nitride ceramics have good insulation and thermal conductivity and are ideal semiconductor packaging materials. They need to be coated with a metal layer (metallization) to prepare the circuit [1–5]. Laser-activated aluminum nitride ceramic metallization utilizes laser shock to form an aluminum layer on the surface of aluminum nitride, followed by chemical copper coating to prepare conductive circuits. It is a promising method of directly preparing circuits on heteromorph devices [6–8].

However, the melting point of aluminum nitride is 2700 °C higher than that of aluminum, which is only 600 °C, making it difficult to control the quality of laser activation

stably. Research on laser activation is still ongoing. Esrom et al. [9,10] used ArF (193 nm), KrF (248 nm), and XeF (351 nm) excimer lasers to process AlN ceramics in air, resulting in aluminum layers with resistivities of 1.65×10^{-7} , 1.03×10^{-7} , and $0.64 \times 10^{-7} \Omega \cdot \text{m}$, respectively. Yung et al. [11] observed and reported on the through-hole circuit of an aluminum nitride substrate prepared by chemical copper plating after laser activation and studied the relationship between laser activation quality and laser wavelength, energy density, repetition frequency, and repeating times. Hirayama et al. [12] measured the electrical resistivity of the AlN sample surfaces after laser activation. The proper conditions for excimer laser micromachining of AlN were also investigated, and comparisons between the two different laser wavelengths (193 nm, 248 nm) used were made. Yang et al. [13] studied the resistance of an Al layer with nanosecond laser activation on an AlN ceramic. They found the resistance is inversely proportional to the duration of the pulse in the case of low energy density, and the resistance is proportional to the duration of the pulse in the case of higher energy density.

The effect of the air bath environment is also an interesting topic [14,15]. Cao et al. [16] studied the oxidation behavior of AlN ceramics under an air atmosphere and found that the AlN ceramic surface became rough, porous, and cracked, leading to a sharp drop in the flexural strength and thermal conductivity of the AlN ceramics at 1200 °C and higher. Morita et al. [17] conducted chemical nickel plating on the surface of aluminum nitride after laser activation metallization and used laser shocking on the surface of aluminum nitride in an argon environment to obtain a minimum resistivity of $2.5 \times 10^{-7} \Omega \cdot \text{m}$. After nickel plating, the resistivity of the metal wire decreased to $1 \times 10^{-7} \Omega \cdot \text{m}$. Kozioł et al. [18–20] prepared conductive aluminum paths on aluminum nitride ceramics in three gas bath environments using the laser activation method. They found that the path resistance decreased with increasing energy density, and the resistance values in various gas bath environments went in the descending order of argon, nitrogen, and air.

Although laser activation will generate a wider metal layer in an argon environment than nitrogen and air, these data are very imprecise. Usually, laser energy density is used to describe this processing difference. However, the existing concept of laser energy density is an average value and is not suitable for the threshold of laser activation, because the intensity gradient of the focused Gaussian beam is large, and different intensity distributions represent different energy levels. Here, a precise concept of laser energy density that sees it as being proportional to light intensity is applied to quantitatively evaluate this difference from a new perspective.

2. Experiment of Laser Activation on Aluminum Nitride Ceramics in Various Gas Bath Environments

The laser activation experiment was carried out in various gas bath environments: air, argon, and nitrogen. The same setup was applied as described in Figure 1 of [17]. The experiment used a galvanometer to control the focused laser beam and scan along a straight line on the surface of aluminum nitride at a certain speed. Nitrogen and argon were statically enclosed in the chamber. When processing was carried out in the air, the chamber was opened, but the window glass was still left in the optical path. The beam was focused on the AlN ceramic surface. Therefore, the morphology of aluminum nitride ceramics after laser activation could be observed with the KEYENCE confocal microscope VK-X1000 equipment came from Shanghai Keyence Co., Ltd., Shanghai, China, at a resolution of 1 nm with a 50× objective lens.

In the experiment, the laser power was set as 20 W, and the scanning speed was adjusted to 500 mm/s according to the repetition frequency of 50 kHz, with a wavelength of 1064 nm and a focal length of 254 mm. There were differences in the metalized line generated by the laser shock under the same processing parameters but in three different gas environments. The width of the metalized line was measured with the confocal microscope. The microscopic image and three-dimensional morphology of laser-activated aluminum nitride ceramics under three gas environments are shown in Figure 1.

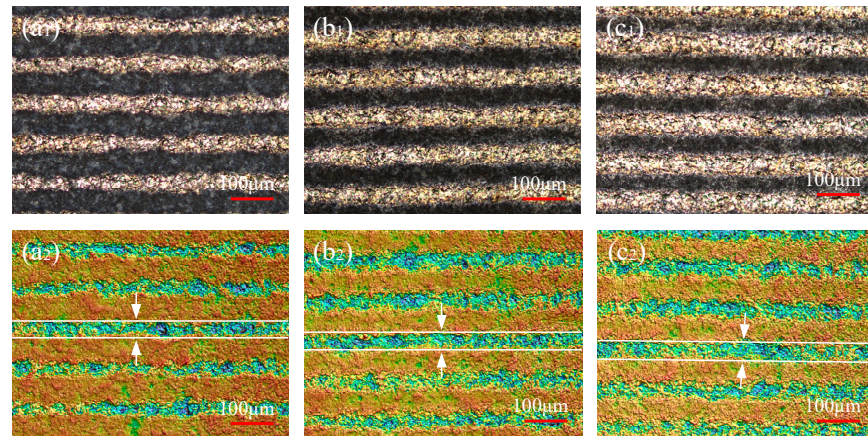


Figure 1. Morphology of laser-activated aluminum nitride ceramics: (a1) microscopic image under air; (a2) 3D morphology under air; (b1) microscopic image under argon gas; (b2) 3D morphology under argon gas; (c1) microscopic image under nitrogen gas; (c2) 3D morphology under nitrogen gas.

In Figure 1(a1–c1), the yellow lines are the aluminum line produced by the laser activation, and the corresponding 3D morphology is shown in Figure 1(a2–c2). According to the depth of the groove generated by laser processing, there was a color change in the morphology. To reduce errors, the average of five measurements was taken as the width of the metalized line. The widths of the metalized lines in air, argon, and nitrogen were obtained as 40.11 μm , 46.21 μm , and 44.87 μm , respectively. This is consistent with the findings of [18–20].

However, this paper cannot delve into the laser processing process to describe the subtle differences in micro-morphology. Additionally, the laser energy density determines the energy required for the laser activation of aluminum nitride ceramics and is a key parameter in the laser processing process. Unfortunately, the existing method for calculating laser energy density calculates the average energy density, which is not suitable. Here, a precise laser energy density proportional to the intensity distribution was applied to accurately represent the subtle energy density difference required for the laser activation of aluminum nitride ceramics in different gas environments. In addition, due to the excessive concentration of energy in the focused laser beam, which would have destroyed the detector, the distribution of intensity could not be directly obtained. Therefore, it is proposed that the intensity distribution of the focused laser beam be indirectly obtained from the intensity distribution of the incident collimated Gaussian beam.

3. Method of Calculating Laser Energy Density Based on the Intensity Distribution of a Focused Laser Beam

Aluminum nitride ceramics are very sensitive to laser parameters and require strict control of the laser parameters in laser activation processing [20,21]. The laser energy density can determine the energy required for laser activation, which is a key parameter for describing the laser processing process. The calculation for laser energy density is normally described as

$$\bar{\psi} = \frac{4P}{\pi D^2 f_{rep}}, \quad (1)$$

where P is the laser power, D is the diameter of the laser-focused spot, and f_{rep} is the repetition frequency. Formula (1) shows an average laser energy density. However, the beam generated from the laser belongs to a Gaussian beam, and the energy density varies at different positions. If the average energy density is used as the laser energy density, there will be significant errors, and the energy required for the laser activation of aluminum nitride ceramics cannot be accurately determined. Therefore, it is necessary to determine a high-precision method for calculating the energy density corresponding to the intensity distribution of the focused laser beam.

It is necessary to obtain the intensity distribution of the focused beam, which is too strong to be directly measured. However, the intensity distribution of the focused beam can be indirectly obtained by using the intensity distribution of the collimated incident beam. In Fourier optics theory, the relationship between the light field distribution of the focused beam (focal plane) and the light field of the collimated beam (pupil plane) can be expressed as a Fourier transform [22,23]:

$$\begin{aligned} U(x, y) &= \frac{1}{\pi} \iint_{u^2+v^2 \leq 1} A(u, v) \exp[i(u^2 + v^2)f + i\Phi(u, v)] \\ &\quad \times \exp(2\pi iux + 2\pi ivy) dudv \\ &= \mathcal{F}\{A(u, v) \exp[i(u^2 + v^2)f + i\Phi(u, v)]\} \\ &= \mathcal{F}\{P(u, v)\} \end{aligned} \quad (2)$$

where $U(x, y)$ is the field function; x and y are the Cartesian coordinates of the focal plane; $A(u, v)$ is the amplitude function on the pupil plane; $\Phi(u, v)$ is the phase function on the pupil plane; $P(u, v)$ is the complex function on the pupil plane; u and v are the normalized coordinates of the pupil plane; f is the defocusing amount; and \mathcal{F} is the Fourier transform marker.

The experiment used a fiber laser, which was coupled and output by fibers, while the amplitude distribution of fiber diffraction was uneven. In research on point diffraction interferometers, fiber diffraction has been shown to generate an approximately ideal spherical wave. The spherical wave is converted into a collimated beam through a long focal length collimator, which can be used as an ideal optical system. The wavefront of a collimated beam can be approximated as an ideal plane wave.

Therefore, in Formula (2), $f = 0$, $\Phi(u, v) < 1/10\lambda$, which can be ignored, so the light field can be approximated as the Fourier transform of $A(u, v)$, namely:

$$U(x, y) = \mathcal{F}\{A(u, v)\} \quad (3)$$

In Formula (3), $A(u, v)$ is the amplitude distribution of the collimated beam converted from the diffraction spherical light field through a collimator, which is a non-uniform light field distribution. In this article, $A(u, v)$ was obtained from the intensity distribution of the collimated fiber laser beam captured with a camera, as shown in Figure 2 (which is different from [24], where the information on the collimated beam only comes from the beam diameter). Then, the mathematical model was built. The intensity distribution of the focused beam can be expressed as

$$I(x, y) = |U(x, y)|^2 \quad (4)$$

where $I(x, y)$ is the intensity of the focused beam; $U(x, y)$ is the complex function of the focal field.

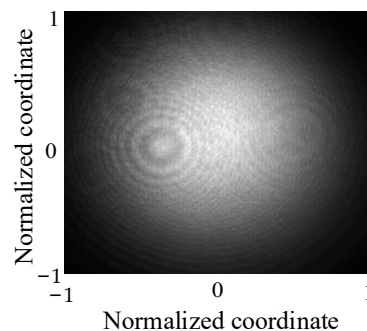


Figure 2. The intensity distribution of a collimated laser beam captured with a camera.

Figure 3a shows the normalized intensity of the focused laser spot obtained from the collimated beam intensity distribution, which is shown in Figure 2. This calculation process

has been previously successfully used in complex modulation beam shaping research [25]. The cross-section of the focused beam intensity distribution is shown in Figure 3b, and the corresponding normalized intensity provides data for the calculation of laser energy density. Light intensity is directly proportional to energy density. The wider groove edge corresponds to lower light intensity, indicating the need for lower laser energy density.

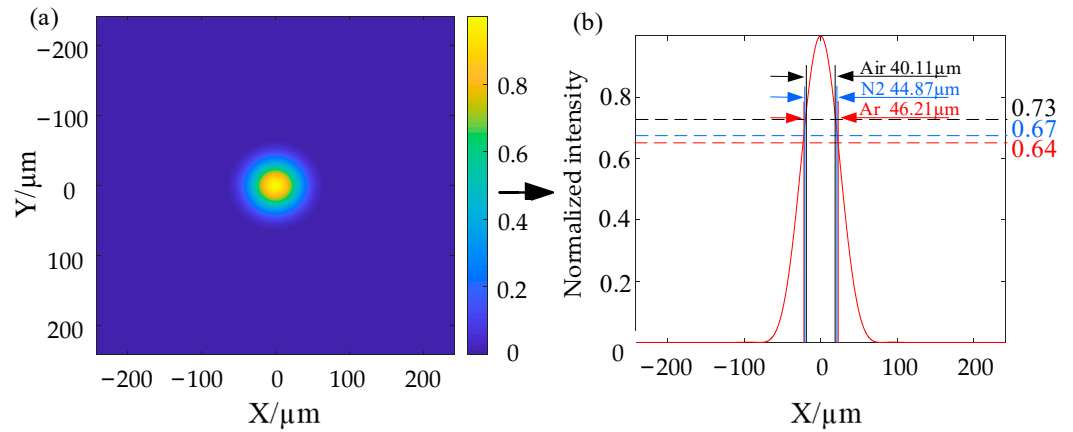


Figure 3. The intensity distribution analysis: (a) normalized intensity distribution of a focused laser beam; (b) cross-section of the intensity distribution.

Due to the proportional relationship between the focused intensity and the laser power, the total intensity of the focused beam ΣI and the average power \bar{P} are certain. By calculating proportionally, the laser power P_1 corresponding to the total intensity of the central region ΣI_1 can be obtained as [24]

$$P_1 = \frac{\bar{P} \times \Sigma I_1}{\Sigma I} \tag{5}$$

Furthermore, based on the beam intensity distribution, the laser energy density in this region is obtained:

$$\psi_1 = \frac{P_1}{S_1 f_{rep}}, \tag{6}$$

where ψ_1 is the corresponding laser energy density; S_1 is the spot area of the region (this is calculated based on the width of the groove formed by laser activation); f_{rep} is the repetition frequency of the laser pulses. The average intensity corresponding to the focused laser beam is \bar{I}_1 . Therefore, the laser energy density corresponding to different intensity distributions is calculated as

$$\psi(x, y) = \frac{\psi_1 \times I(x, y)}{\bar{I}_1}, \tag{7}$$

where \bar{I}_1 is the average intensity in the corresponding central region.

According to Formulas (4)–(7), the laser energy density corresponding to the light intensity at the metalized line edge can be obtained. This value is the threshold of laser energy density required for laser activation. Here, the central region was set as a circle region with a diameter of 40.11 μm (the air gas bath).

4. Calculation of Multiple-Pulse Energy Density for Laser Activation on Aluminum Nitride Ceramics

In actual production processes, it is common to use overlapping adjacent pulses and multiple laser pulses that act together to accumulate enough energy to generate the metalized line (Al), as shown in Figure 4a. Therefore, the energy density calculation should fit this multi-pulse case. As the repetition frequency is fixed, the amount of accumulated

energy of the laser pulse depends on the laser power and laser scanning speed, while the laser scanning speed determines the adjacent laser pulse distance.

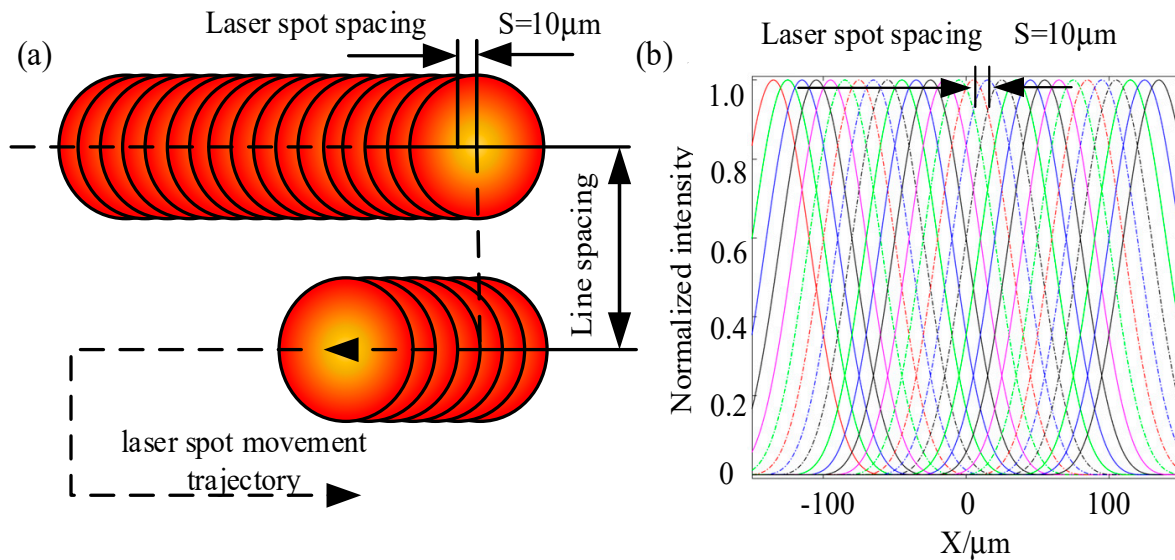


Figure 4. Schematic diagram of multi-pulse laser processing: (a) laser spot movement trajectory and overlap; (b) normalized light intensity cross-section of the overlapping laser spots.

A schematic diagram of multi-pulse laser processing is shown in Figure 4. Figure 4a shows the movement trajectory and overlap diagram of the multiple pulses. To avoid interference between the upper and lower rows, the line spacing is set to be greater than the diameter of the laser spot. Figure 4b shows the normalized light intensity cross-section along the movement trajectory where the laser spot overlaps. The formula for calculating the distance d between two adjacent laser spots is $d = v/f_{rep}$, where v is the laser scanning speed and f_{rep} is the laser pulse repetition frequency. The spacing between the adjacent spots was calculated as $10 \mu\text{m}$.

The analysis result for the multi-pulse accumulated energy density is shown in Figure 5. Figure 5a describes the cumulative intensity distribution of the normalized laser pulse (as shown in Figure 3a) after it moved 50 times along the laser scanning line. Figure 5b shows the cross-section of the cumulative intensity distribution. It can be seen that the central curve is stable, and this means the central data are sufficiently accurate for intensity calculation. Figure 5c shows the cross-section of the cumulative pulse perpendicular to the direction of spot movement at the abscissa position of $0 \mu\text{m}$. The maximum intensity of the accumulated pulse was 6.01. The curve in Figure 5c was used for the energy density calculation. The edge of the metalized line formed by the laser shock means that the energy density here was just enough to cause the aluminum nitride ceramic to decompose into an aluminum layer.

Then, based on the width of the metalized line, the minimum energy density needed for the laser activation of aluminum nitride ceramics in three different gas environments could be obtained. The cumulative normalized light intensities of the metalized line edge in the air, argon, and nitrogen environments were 4.25, 3.78, and 3.88. By introducing the corresponding normalized light intensity into Formula (7), the minimum cumulative energy densities of laser activation in the air, argon, and nitrogen environments could be calculated as 48.2 J/cm^2 , 42.8 J/cm^2 , and 44.0 J/cm^2 , respectively.

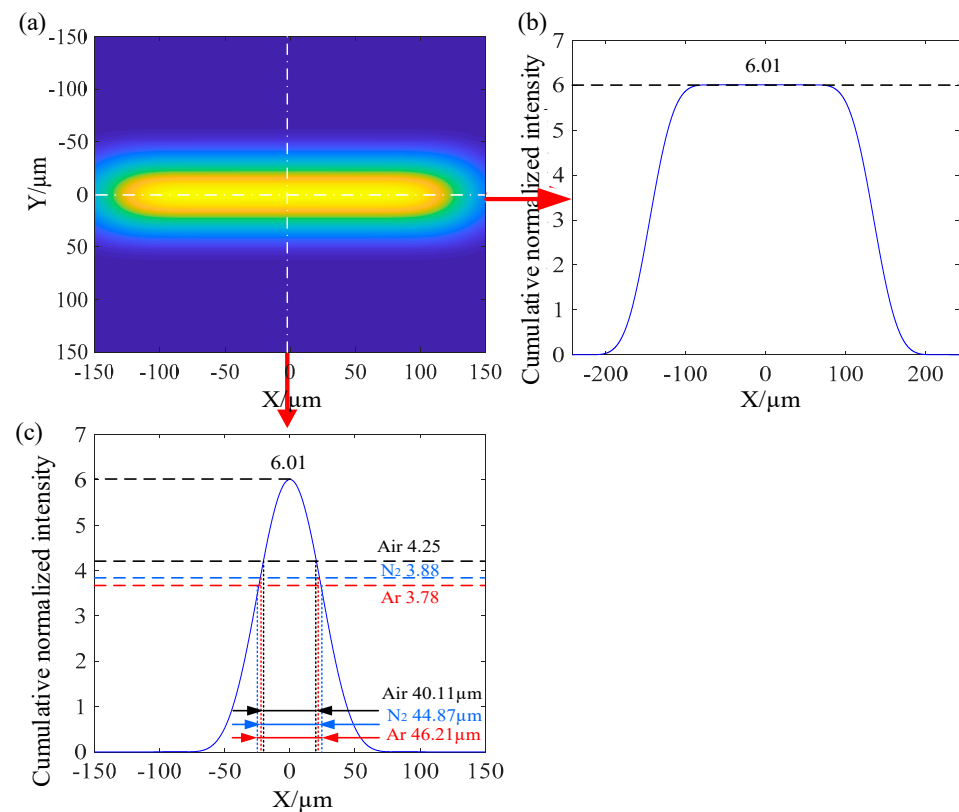


Figure 5. Analysis of accumulated laser energy: (a) the accumulated intensity distribution from a limited number of normalized single-pulse intensities overlapping; (b) cross-section of laser intensity distribution in the horizontal direction of spot movement; (c) cross-section of laser intensity distribution in the vertical direction of spot movement.

5. Discussion

The above data were calculated based on the line width processed in the air gas bath. When the line widths processed in the other gas baths were used, the deviation was less than 0.2 J/cm^2 . The error may be due to the resolution of the focused beam intensity distribution (the lateral resolution was $0.1 \mu\text{m}$).

In [24], the energy required to form a uniform metal layer was determined to be $21.53 \text{ J/cm}^2 \sim 26.02 \text{ J/cm}^2$, which differs from what was found in this paper. This deviation may be due to the inaccurate estimation of the collimated beam intensity distribution. But this was not the main cause. Another important reason was the diverse repetition frequencies of laser processing, which were 200 kHz [24] and 50 kHz (this article). Higher repetition frequencies lead to higher heat accumulation, resulting in a higher surface temperature of the aluminum nitride ceramic to be processed and a decrease in the laser energy required. This is a unique phenomenon that is different from previous literature descriptions.

If the processing parameters can be controlled correctly, laser activation under different gas baths only causes changes in the conductivity and line width of the metal layer [18,19,26]. Based on the minimum cumulative energy densities of laser activation in the air, argon, and nitrogen environments, it was found that different laser energy densities are required for processing under different gas baths. Further research will focus on investigating how the differences in energy density affect the microstructure.

6. Conclusions

Laser processing uses a Gaussian beam, which has large variation in laser energy density. Therefore, for Gaussian beams, the existing laser energy density is an average value. This laser energy density is not accurate enough for researching the difference in laser energy required for aluminum nitride ceramics under different gas baths. This article

uses a concept of laser energy density that sees it as being proportional to the intensity distribution. However, due to the excessive concentration of energy in a focused laser beam, which will destroy the detector, the intensity distribution is hardly directly obtained. Here, the intensity distribution of a focused laser beam was indirectly obtained from the intensity distribution of the incident collimated Gaussian beam, which was captured with a camera. It was found that the minimum energy density in air increases by 12.5%, and the minimum energy density in nitrogen increases by 3%, using the minimum energy density required for laser activation in argon gas as the reference. Therefore, considering the complexity, low safety, and cost of the equipment, it is believed that laser activation in the air is acceptable under strict control of the laser parameters.

Author Contributions: Conceptualization, J.S. and S.S.; data curation: J.S. and S.H.; formal analysis, H.Z.; investigation, H.Z.; methodology, H.Z., J.S. and Z.N.; resources, S.H., P.S. and Z.S.; validation, Z.N. and C.X.; acquisition, H.Z., Y.W. and H.D.; writing—original draft, H.Z. All authors have read and agreed to the published version of the manuscript.

Funding: This research was funded Key Technology Research and Development Program of Shandong (Grant No. 2019GGX104106, No. 2019JZZY010402), China Postdoctoral Science Foundation (Grant No. 2018M632639), Higher Education Discipline Innovation Project—the 111 plan (Grant No. D21017), National Natural Science Foundation of China (Grant No. 51605239).

Institutional Review Board Statement: Not applicable.

Informed Consent Statement: Not applicable.

Data Availability Statement: Data are contained within the article.

Conflicts of Interest: Author Ping Song was employed by the company Ceyear Technologies Co., Ltd. The remaining authors declare that the research was conducted in the absence of any commercial or financial relationships that could be construed as a potential conflict of interest.

References

1. Jiang, H.; Wang, X.; Fan, G.; Fu, M.; Lei, W.; Wang, X.; Liang, F.; Lu, W. Effect of oxidation on flexural strength and thermal properties of AlN ceramics with residual stress and impedance spectroscopy analysis of defects and impurities. *Ceram. Int.* **2019**, *45*, 13019–13023. [[CrossRef](#)]
2. Khazaka, R.; Mendizabal, L.; Henry, D.; Hanna, R. Survey of high-temperature reliability of power electronics packaging components. *IEEE Trans. Power Electron.* **2015**, *30*, 2456–2464. [[CrossRef](#)]
3. Miyazakia, H.; Iwakiri, S.; Hirao, K.; Fukuda, S.; Izu, N.; Yoshizawa, Y.I.; Hyuga, H. Effect of high temperature cycling on both crack formation in ceramics and delamination of copper layers in silicon nitride active metal brazing substrates. *Ceram. Int.* **2017**, *43*, 5080–5088. [[CrossRef](#)]
4. Arabi, F.; Theolier, L.; Martineau, D.; Deletage, J.Y.; Medina, M.; Woirdard, E. Thermo-mechanical reliability assessment of AlN power substrates subjected to severe aging tests. *Mater. Focus* **2017**, *6*, 352–358. [[CrossRef](#)]
5. Nedyalkov, N.; Dilova, T.; Dikovska, A.; Nikov, R.; Nikov, R.; Koleva, M.; Stankova, N.; Daskalova, A.; Angelova, L. Laser processing of nitride ceramics. *J. Phys. Conf. Ser.* **2022**, *2240*, 012044. [[CrossRef](#)]
6. Nedyalkov, N.; Dikovska, A.; Nikov, R.; Nikov, R.; Dliova, T.; Atanasova, G.; Aleksandrov, L.; Karashanova, D.; Strijkova, V.; Terakawa, M. Nanosecond laser-induced oriented periodic structures on AlN ceramic. *Appl. Surf. Sci.* **2022**, *585*, 152712. [[CrossRef](#)]
7. Liu, D.; Chen, N.; Song, Y.; Song, X.; Sun, J.; Tan, C.; Long, W.; Zhong, S.; Jia, L. Mechanical and heat transfer properties of AlN/Cu joints based on nanosecond laser-induced metallization. *J. Eur. Ceram. Soc.* **2023**, *43*, 1897–1903. [[CrossRef](#)]
8. Chen, N.; Chen, B.; Liu, D.; Song, Y.; Zhu, H.; Song, X.; Tan, C. Joining of nanosecond laser irradiation modified-AlN and Cu. *Ceram. Int.* **2021**, *47*, 27979–27986. [[CrossRef](#)]
9. Esrom, H.; Zhang, J.Y.; Pedraza, A.J. Excimer Laser-Induced Decomposition of Aluminum Nitride. *MRS Proc.* **1991**, *236*, 383. [[CrossRef](#)]
10. Pedraza, A.J.; Zhang, J.Y.; Esrom, H. Surface Modification of Aluminum Nitride and of Aluminum by Excimer Laser. *MRS Proc.* **1992**, *285*, 209. [[CrossRef](#)]
11. Yung, K.C.; Chen, C.; Lee, C.P. Laser induced activation of circuit lines and via-holes on AlN for electroless metal plating. *Appl. Surf. Sci.* **2011**, *257*, 6601–6606. [[CrossRef](#)]
12. Hirayama, Y.; Yabe, H.; Obara, M. Selective ablation of AlN ceramic using femtosecond, nanosecond, and microsecond pulsed laser. *J. Appl. Phys.* **2001**, *89*, 2943–2949. [[CrossRef](#)]

13. Yang, Q.; Chen, Y.; Lv, Z.; Chen, L.; Lou, D.; Zheng, Z.; Cheng, J.; Liu, D. Nanosecond laser surface processing of AlN ceramics. *J. Mater. Sci.* **2019**, *54*, 13874–13882. [[CrossRef](#)]
14. Yabe, H.; Takahashi, A.; Sumiyoshi, T.; Obara, M.; Ishii, K. Direct Writing of Conductive Aluminum Line on Aluminum Nitride Ceramics by Transversely Excited Atmospheric CO₂ Laser. *Appl. Phys. Lett.* **1997**, *71*, 2758–2760. [[CrossRef](#)]
15. Nicolas, G.; Autric, M. Production of a Metallic Thin Film on AlN Surface by UV Laser Radiation. *Appl. Surf. Sci.* **1997**, *109/110*, 477–481. [[CrossRef](#)]
16. Cao, C.; Feng, Y.; Qiu, T.; Yang, J.; Li, X.; Liang, T.; Li, J. Effects of isothermal annealing on the oxidation behavior, mechanical and thermal properties of AlN ceramics. *Ceram. Int.* **2017**, *43*, 9334–9342. [[CrossRef](#)]
17. Morita, N.; Watanabe, T.; Yoshida, Y. Direct Formation of Conductor Films by Laser Sublimating of Ceramics. *Appl. Phys. Lett.* **1989**, *54*, 1974–1975. [[CrossRef](#)]
18. Koziół, P.E.; Antończak, A.J.; Szymczyk, P.; Stępak, B.; Abramska, K.M. Conductive aluminum line formation on aluminum nitride surface by infrared nanosecond laser. *Appl. Surf. Sci.* **2013**, *287*, 165–171. [[CrossRef](#)]
19. Koziół, P.E.; Górski, P.A.; Byndas, A.; Antończak, A.J.; Stępak, B.D.; Abramski, K.M. Experimental verification of the method for producing a three-dimensional cross-pairs metamaterial structure based on a dielectric AlN cube. *J. Phys. D Appl. Phys.* **2016**, *49*, 065104. [[CrossRef](#)]
20. Antończak, A.J.; Koziół, P.E.; Stępak, B.; Abramski, K.M. Direct selective metallization of AlN ceramics induced by laser radiation. In *Laser-Based Micro-and Nanoprocessing VIII*; SPIE: Bellingham, DC, USA, 2014; Volume 8968, pp. 214–223.
21. Shao, J.; Dong, H.; Zhang, R.; Wang, Y.; Han, S. Effect of laser parameters and atmosphere in the structuring of aluminum nitride. *Appl. Ceram. Technol.* **2022**, *19*, 3040–3048. [[CrossRef](#)]
22. Goodman, J.W. *Introduction to Fourier Optics*; McGraw-Hill: New York, NY, USA, 1968.
23. Han, C.Y. *Fundamental Theory and Application of Information Optics*; Changchun Press: Changchun, China, 1989.
24. Shao, J.; Zhang, R.; Han, S.; Dong, H.; Sun, S. The activation threshold evaluation of metalization for aluminum nitride ceramic under nanosecond laser pulses in air. *Ceram. Int.* **2021**, *47*, 24707–24712. [[CrossRef](#)]
25. Shao, J.; Haase, T.; Zhang, R.; Agueraray, C.; Broderick, N.; Sun, S. Focusing flattop beam shaping with complex modulation holography. *AIP Adv.* **2021**, *11*, 105118. [[CrossRef](#)]
26. Shao, J.; Wang, Y.; Zhu, K.; Sun, Z.; Han, S.; Dong, H.; Sun, S.; Song, P.; Zhang, R. Interface stress analysis and bonding strengthening exploration of metal layer on the laser-activated copper-clad AlN. *Microelectron. Reliab.* **2024**, *155*, 115369. [[CrossRef](#)]

Disclaimer/Publisher’s Note: The statements, opinions and data contained in all publications are solely those of the individual author(s) and contributor(s) and not of MDPI and/or the editor(s). MDPI and/or the editor(s) disclaim responsibility for any injury to people or property resulting from any ideas, methods, instructions or products referred to in the content.